Mecánica Computacional Vol. XXIV
A. Larreteguy (Editor)
Buenos Aires, Argentina, Noviembre 2005

COMPUTATION OF THE FREE SURFACE FLOW IN A FISH PASSAGE

Pablo M. Carrica, Cagri Turan and Larry Weber

IIHR-Hydroscience and Engineering
The University of Iowa
Iowa City, IA 52242
Pablo-carrica@uiowa.edu

Key words: Free surface flows, environmental flows, fish passage, VOF.

Abstract. *A numerical study of the free surface flow on an ogee-crested fish bypass is presented. The geometry corresponds to a juvenile fish bypass proposed for Wanapum Dam, on the Columbia River, State of Washington. A free-surface numerical model which solves the RANS equations coupled to a surface-capturing algorithm to predict the flow in air and water was developed using the volume of fluid (VOF) method with the commercial CFD code Fluent 6.1. The* $k-\varepsilon$ *model of turbulence with wall functions was used to compute the eddy viscosity. Structured/unstructured hybrid grids were used to accommodate the complex geometry that included gate slots, flow control gates, and an aeration slot. The tailrace performance curves were reproduced numerically, predicting the plunging, skimming or surface ramp regimes resulting from different tailrace elevations. Free surface elevations, pressure along the ogee surface, and discharge rating curves were compared against the experimental data from the laboratory model for different headwater elevations and gate settings. Once deemed reliable through validation against experimental data, the computational model was used to analyze the flow field, supplementing the areas of limited experimental data. Predicted numerical model results included pressure and velocity distributions and free-surface configurations that helped analyze cavitation potential and flow performance of the spillway. Future analysis may link the hydrodynamic results with an existing fish behavioral model.*

1 INTRODUCTION

Hydropower installations have produced a number of benefits such as renewable and non-polluting energy generation, flood control, navigation conditions, irrigation, and water supply. However, they have also contributed to the decline of the anadromous fish population in the Columbia River[1]. The negative impact of hydropower dams on the fish population is well known and has resulted in the focus of regulatory agencies to promote development of better fish passage facilities with minimal mortality at hydropower dams[2].

Numerical methods applied to these types of problems can assume or compute a free surface shape. Free surface calculations give more information about flow characteristics but require more highly complex algorithms and grids. In this context, surface tracking and surface capturing methods have been applied to hydraulics problems. Surface tracking methods deform the grid to fit the free surface, which simplifies the implementation of the boundary conditions at the free surface but limits its application to relatively simple free surface topologies. Among other hydraulics applications, this method has been used for the computation of channel[3] and spillway flows[4]. Surface capturing methods have the advantage that they can tackle complicated free surface topologies, including air entrainment, spilling and breaking waves, etc. One popular surface capturing method is the Volume of Fluid (VOF) method. A numerical and physical model study for the flow over an ogee-crested spillway was presented in reference 5. The CFD package Flow-3D was used to solve the RANS equations, and the VOF method was used to compute the free surface[6,7]. Chen *et al.*[8] also used the VOF method to simulate flow over a stepped spillway. In both cases, the predictions were compared against experimental data and showed good agreement.

In this study we present numerical results for an ogee-crested spillway which will be used as a fish passage route from the forebay to the tailrace at Wanapum Dam on the Columbia River, Washington State. The VOF method available in Fluent 6.1 was used to model the free surface flow through the fish bypass. The study showed that commercial numerical tools are capable of analyzing many aspects of free surface flows occurring in hydraulic engineering applications. The complex geometry of the fish bypass was modeled using hybrid structured/unstructured grids. The model was extensively validated against experimental data for flow rates at different headwater elevations and gate settings, free surface elevations, and pressure distribution at the ogee surface. Once proven accurate, the numerical model was used to calculate information, including pressure and velocity distributions, that were not available with the experimental model. This information guided the design to avoid cavitation damage through aeration, to analyze inlet conditions in order to help predict the efficiency for fish capture, and to study fish stress at different locations on the spillway.

2 CFD MODELING APPROACH

The fish bypass was analyzed using the commercial CFD code Fluent 6.1[9]. The following section describes the mathematical and numerical models used, as well as grid design considerations and boundary conditions.

2.1 Mathematical model

The flow was assumed to consist of a two-phase incompressible mixture of air and water. Air was considered incompressible as well, a valid approximation at model scale. It has been argued that on the field scale tailrace, bubbles at relatively high depth will experience considerable pressure (less than 3 atm maximum at Wanapum Dam). However, this study was not concerned with computation of bubble entrainment, and air was therefore only of interest at the air water interface. The Reynolds-Averaged Navier-Stokes (RANS) equations govern the fluid motion subject to the continuity constraint:

$$\frac{\partial(\rho \mathbf{v})}{\partial t} + \nabla \cdot (\rho \mathbf{v}\,\mathbf{v}) = -\nabla p + \nabla \cdot \left[\mu_{eff} (\nabla \mathbf{v} + \nabla \mathbf{v}^T) \right] + \rho \mathbf{g} \tag{1}$$

$$\nabla \cdot \mathbf{v} = 0 \tag{2}$$

where the effective viscosity is defined as:

$$\mu_{eff} = \mu + \mu_t \tag{3}$$

with the turbulent viscosity, μ_t, computed from a standard $k-\varepsilon$ model:

$$\mu_t = C_\mu \frac{k^2}{\varepsilon} \tag{4}$$

Eqs. (1) and (2) are valid within each fluid, with the density, ρ, and viscosity, μ, constant for each fluid. At the air/water interface, mass and momentum jump conditions apply.

2.2 Free surface

Fluent 6.1 models the free surface using a Volume of Fluid (VOF) method[6,7]. In the VOF model, the interface between fluids is found using a volume fraction equation. Mass conservation on the water phase requires:

$$\frac{\partial \alpha_w}{\partial t} + \mathbf{v} \cdot \nabla \alpha_w = 0 \tag{5}$$

and the constraint that cells can only be occupied by each fluid or a mixture of fluids requires $\alpha_w + \alpha_a = 1$. The solution of Eq. (5) is performed using a reconstruction-transport algorithm that keeps the interface sharp while conserving the volumes of air and water invariant. This is important because it overcomes the main weakness of other interface capturing methods, in particular the level set method (see Sethian and Smereka[10] for a discussion on the subject). The major drawback of VOF methods lies in the difficulty of computing normals and curvatures. Since in this application we neglect surface tension effects, this does not apply to our case. Thus, points in water have $\alpha_w = 1$, points in air $\alpha_w = 0$, and points near the interface will have $0 < \alpha_w < 1$. The jump conditions across the interface are embedded in the model by defining the fluid properties as:

$$\phi = \phi_w \alpha_w + \phi_a \left(1 - \alpha_w\right) \tag{6}$$

where ϕ is either density or viscosity. Other interfacial phenomena such as surface tension effects can be added as volume forces, if needed. Since the scale of modeling is large, and small scale details of the flow such as spray or bubble formation are of no interest, we can safely neglect surface tension. Moreover, direct numerical simulation of the air entrainment process is beyond the capability of modern computers, even at model scale.

2.3 Numerical model

Eqs. (1), (2), and (5) were solved sequentially (the segregated option in Fluent), coupled to a standard model with wall functions for turbulence closure. The continuity equation was enforced using a body force weighted PISO algorithm, resulting in a Poisson equation for the pressure. Unsteady solutions were obtained using a fixed time-step between 0.0005 and 0.002 s. Statistically converged solutions were obtained running typically 20 to 30 s, using the flow rate as convergence parameter.

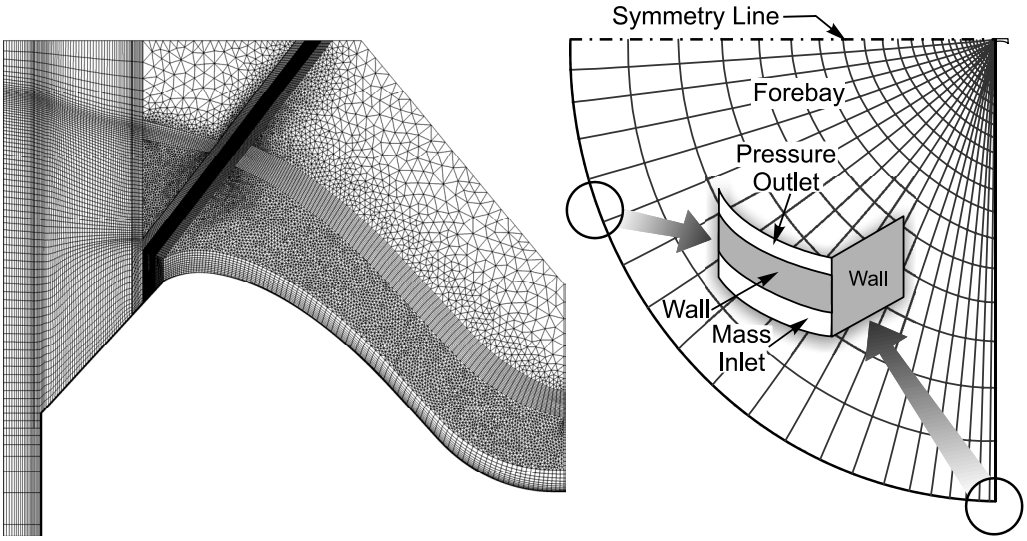

Figure 1: Grid overview and boundary conditions

2.4 Grid design

The grids were generated using Gridgen V15.4. Since the geometry is almost symmetric about the plane, only half of the domain was simulated. Small differences in the forebay geometry on each side of the centerplane and possible non-symmetrical flow instabilities were assumed to be negligible. The close agreement between numerical and experimental data supports this approximation. Hybrid grids, each containing around 1,000,000 nodes, were used for the different forebay and gate scenarios. The grid quality was critical to achieve

convergence. Because it is known that collocated methods have more instability problems on the air/water interface region when using non-orthogonal grids and high aspect ratio[10], nearly orthogonal structured grids with cell aspect ratio smaller than 10 and with expansion ratio no larger than 2 were used wherever possible. Since the geometry was too complex to generate a fully structured grid with good quality (mainly when gates and gate slots are considered), complex geometry regions were generated using unstructured grids in one plane and structured grids in the third direction. For most cases, convergence could not be achieved using fully unstructured grids, presumably due to grid quality issues caused by the available computational processing power, which limited the grid to a little over a million cells.

To resolve regions of interest, the grids were refined at all no-slip conditions, near the gates where large accelerations were found and near the free-surface (critical to obtain good quality results). To properly fit the free surface region with a good quality structured grid, different grids were generated for each case in which the free surface location changed. Side and top views of a sample grid are provided in Fig. 1.

2.5 Boundary conditions

The boundary conditions are discussed referencing Fig. 1. A critical design aspect of the boundary conditions was to achieve a stable flow rate given a headwater elevation. This was accomplished in this study by simulating a very large pool (3000 m in radius) in which the free surface elevation was imposed with an inlet flow condition on the lower far-field forebay boundary. On this boundary, a wall with appropriate elevation separated the inlet flow condition from a pressure outlet boundary condition (at atmospheric pressure) which was used to spill the excess of water that was introduced at the inlet boundary. This effectively controlled the far-field headwater elevation and allowed a stable flow-rate through the bypass. Other simpler boundary conditions were tested with no success to achieve the same goal. Sides and bottom walls were modeled as no-slip everywhere within the bypass. To maintain low turbulence levels at the forebay inlet, slip conditions were used along with zero turbulent kinetic energy at the inlet face. This effectively prevented turbulence production upstream of the bypass entrance. Everywhere at the top, a pressure outlet boundary condition with atmospheric pressure was applied to allow free-air flow and avoid unrealistic air pressurization. A pressure outlet boundary condition is used at the bypass exit since the problem was inertia dominated and there were no recirculation problems.

3 SIMULATION CONDITIONS

The numerical calculations were performed for different headwater elevations and gate settings to control the discharge. The numerical model was constructed at prototype scale in order to obtain valid predicted stresses. Four different headwater elevations were considered, including the normal pool elevation (173.74 m), the highest expected elevation (175.26 m), and two lower elevations (170.69 m and 172.21 m). Design conditions are investigated for free flow (ungated) and with the vertical gate raised, then one, two, or three of the inclined gates inserted within the inclined gate slots, all for headwater elevation 173.74 m. As previously discussed, grid quality requirements forced the use of a specifically designed grid

for each condition. This was achieved by initially running a coarse, high-quality grid to estimate the location of the free surface and then redesigning the grid to match the free-surface location. For all cases, the headwater elevation was fixed by setting the inlet boundary conditions as described in the previous section. The flow rate and the overall free surface topology were then predicted based solely on the operational conditions.

4 VALIDATION

The numerical model was extensively validated against the experimental data taken on the physical model at IIHR. The experimental data was scaled to prototype equivalents (based on Froude scaling laws) and compared to numerical model predictions. Validation included comparing discharge, free surface elevation, and ogee centerline pressure between numerical model and laboratory measurements. Other variables that do not scale (air entrainment and stresses) were not used for validation.

The rating curves combined different headwater elevations and gate settings. Each headwater elevation or gate setting resulted in a converged discharge (to within 0.01%) predicted by the model. Figure 2 shows a comparison between the experimental data and the numerical model predictions. To compute the discharges on the model, the mass flux was integrated in a plane between the fish passage entrance and the gate slots. A key point to obtaining good quality steady-state discharges is the control of the forebay elevation. This was discussed in the Boundary Conditions section, but it is stressed here that standard pressure-inlet conditions result in oscillatory discharges.

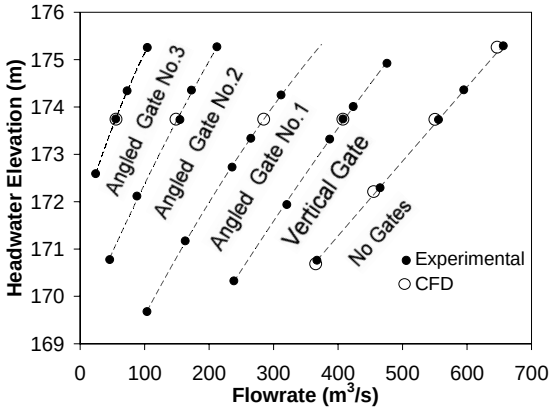

Figure 2: Rating curves for various operating conditions

As seen in Fig. 2, the agreement between the measured and predicted discharges was excellent, with the difference between predicted and measured discharges never exceeding 2 %. These differences were likely due to some approximations made on the numerical model, including the symmetry assumption, the extension of the inlet fairings to the bottom of the forebay, and to small errors in headwater elevation control, caused by the of the spill region

height at the inlet boundary.

Numerically predicted free surface profiles were compared to experimental results for headwater elevations of 173.74 m and 175.26 m for unregulated flow conditions and at headwater elevation of 173.74 m for regulated flow conditions. A strong deflection on the free surface was caused by the gate slots and the air slot, complicating the measurement of the free surface at the side walls of the spillway section. Figure 3 shows the comparisons at headwater elevations of 173.74 m and 175.26 m for unregulated flow, and the free surface elevations at headwater elevation 173.74 m with different gates in place, respectively. The spillway ogee and the gates are shown schematically along with the free surface location. The location of the free surface for the numerical model was set at $\alpha_w = 0.5$. In both cases, the agreement between measured and predicted results was very close.

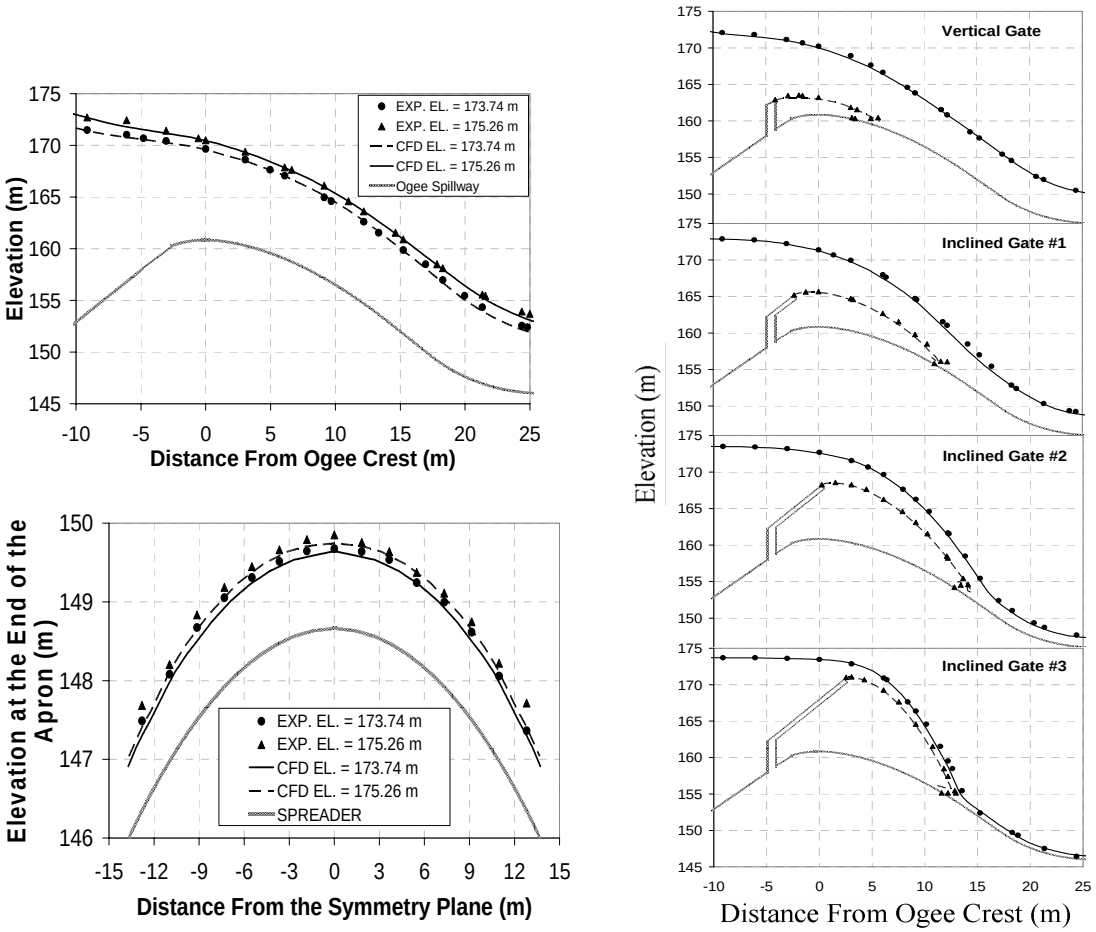

Figure 3: free surface elevations predicted for unregulated conditions (upper left), different regulated conditions (right) and at the end of the spreader (lower left).

Also shown in Fig. 3 is a comparison between numerical predictions and experimental data for the free surface elevation at the bypass exit. The apron was designed to spread the bypass flow uniformly upon discharging to the tailrace, which is reflected in the numerical results. There is a slight non-symmetry in the experimental data which is not reflected in the CFD computations since the centerplane is a symmetry boundary condition. The CFD predictions underestimate the elevation by as much as 15 percent. One possible explanation for this discrepancy is the presence of free surface fluctuations in the experimental model that are not present in the computations, which could lead to detection of the maximum rather than the average free surface elevation. In addition, air entrainment not captured by the numerical model would increase the flowing volume, causing a higher experimental elevation at the exit of the bypass.

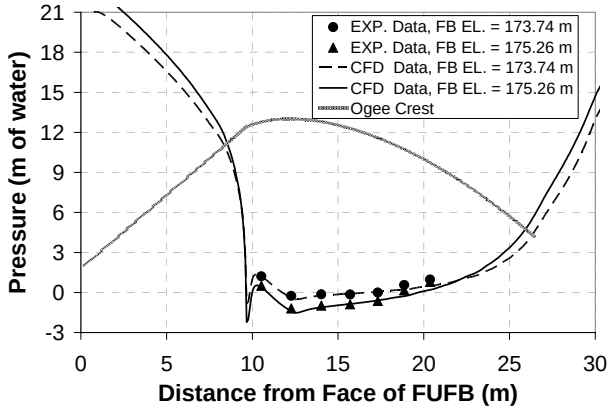

Figure 4: Gage pressures at the ogee symmetry line

The advantage of an ogee crested spillway is its ability to generate low pressure values near the crest. This low pressure promotes a higher discharge efficiency but may also cause cavitation damage as pressures approach the vapor pressure point. An air supply to the ogee increases the surface pressure to values closer to atmospheric pressure and decreases the chance for cavitation to occur. In addition, the compressibility of air will prevent concrete damage from cavity collapse. Numerical gage pressure values at the ogee symmetry line are compared with the experimental results for headwater elevations 173.74 m and 175.26 m in Fig. 4. The minimum measured pressure is accurately predicted with the numerical model. The numerical model detected a localized low pressure peak at the start of the ogee curve upstream of the crest. Extreme care was taken to properly model the ogee shape since the pressure magnitudes were highly sensitive to small changes in curvature in this region.

5 PREDICTED RESULTS

Velocity profiles were analyzed at selected locations. Of special interest were velocity

profiles at the gate slots, since a sudden change in section occurs there that could damage fish if they were attracted to it. Figure 5 shows velocity at lines parallel to the vertical and inclined gate slots at incremental distances from the center plane (y=2.81 is the location of the side wall). Notice that the effect of the gate slots on the velocity profile was restricted to a region about 30 cm away from the slots. The core velocity rapidly developed further out. Figure 6 shows axial velocity at selected cross sections. Note that the developing boundary layer was still thin near the gate slots and grew thicker downstream. The maximum velocity upstream of the crest is located near the free surface, but the maximum velocity shifted to the bottom near the ogee crest. After passing the crest, the maximum velocity was again found at the free surface. Notice that at the gate slots a negative axial velocity developed, indicating the presence of a local flow recirculation.

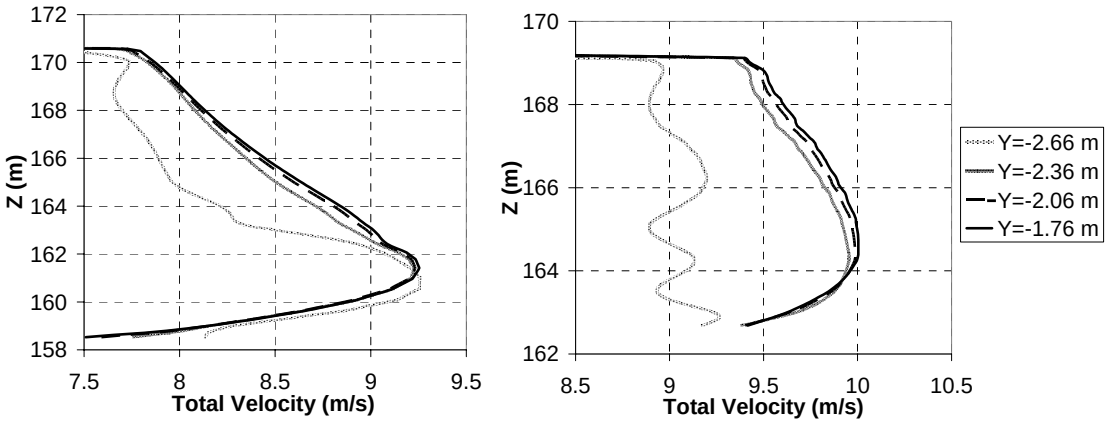

Figure 5: Velocity distribution along the vertical (left) and inclined (right) gate slots

The numerically computed free surface geometry and a close-up of the flow near the gate slots are shown in Fig. 11. The colored ribbons are streamlines on the core of the flow, showing little perturbation by the gate and air slots. The free surface is shown in light blue. Note the free surface deflection on the gate slots caused by strong vortices pushing the fluid down. These vortices are shown with black ribbons. The air slots also entrained air into the flow and had a lower free surface elevation. Numerical predictions of air entrainment were in agreement with experimental observations, though the bubbles predicted by the numerical model were much larger than those entrained in the laboratory. In addition, some air entrainment was observed on the experimental model gate slots that was not predicted by the numerical model. This was a natural consequence of the grid spacing, which was much greater than the model scale bubble size, preventing the numerical model from resolving the bubble evolution.

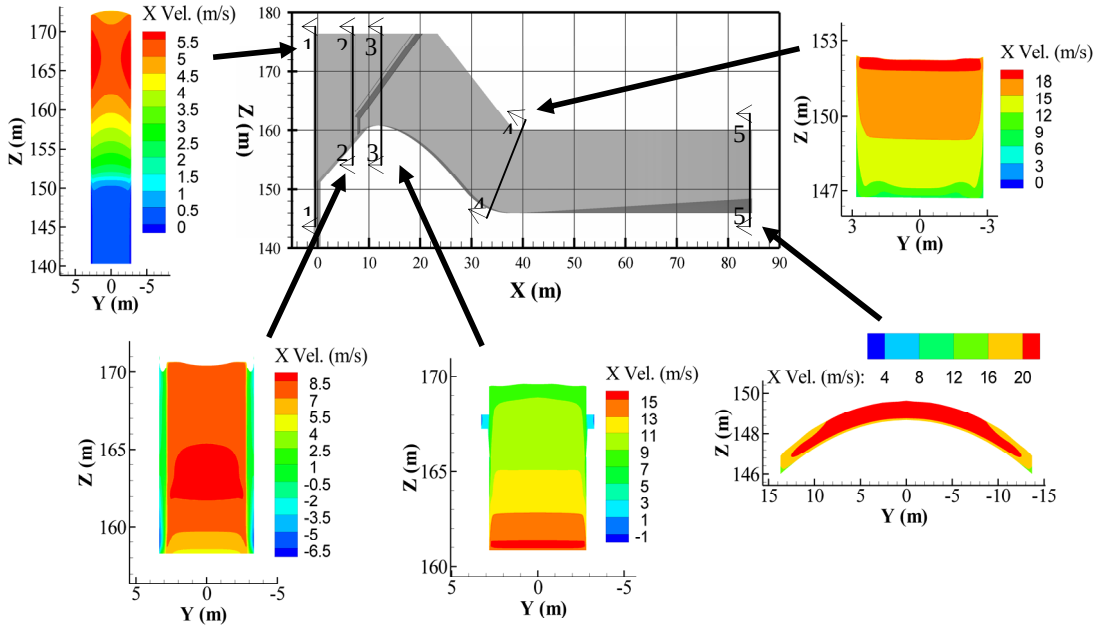

Figure 6: Velocity distribution along at selected cross sections

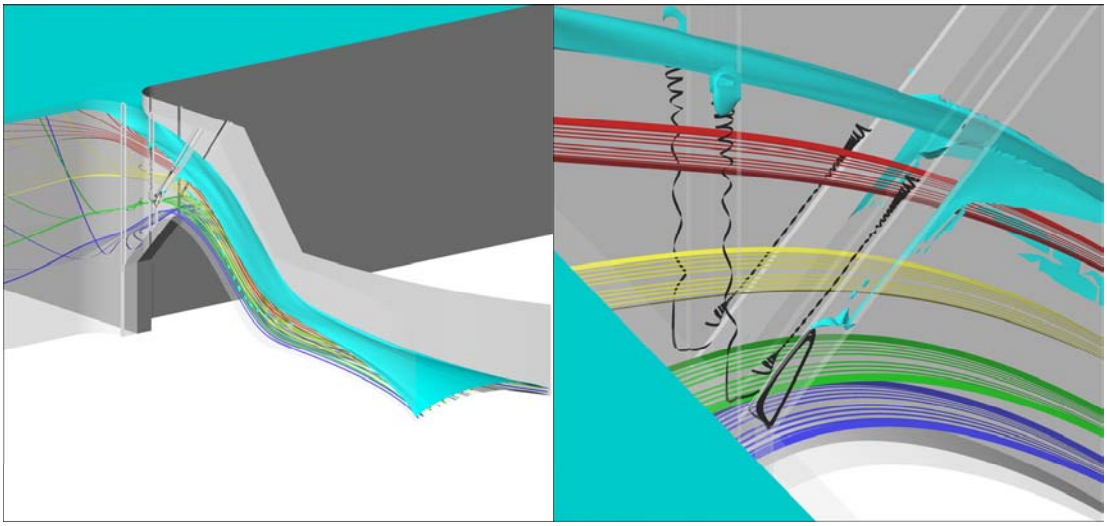

Figure 7: View of the free surface and underlying streamlines

6 CONCLUSIONS

A numerical study of the flow on a fish bypass was presented. The study included free surface elevations, pressure, and discharges measured on a 1:24 scale model of the fish

bypass. A numerical model was developed using Fluent 6.1, including geometry details of gate slots, gates, and an air slot. The numerical model was validated against measured discharges and free surface elevations at two headwater elevations for unregulated flow and at normal pool elevation for regulated flows. Free surface elevation at the end of the bypass exit and pressure distributions along the ogee centerline were also used for validation. The comparison of the numerical model results with experimental data showed excellent agreement. Velocity distributions were evaluated at selected locations and cavitation indexes were also reported, showing that the design did not lead to extreme conditions that might cause cavitation. The free surface numerical model proved to be useful as a design aid tool.

Even at model scale, the air entrainment process was beyond the current capabilities of numerical methods. However, air demand calculations continue to be extremely important, and the development of a model capable of computing the air entrainment would be a natural extension to current numerical simulation capabilities.

7 ACKNOWLEDGEMENTS

The support by Grant County Public Utility District No. 2 of Grant County, Ephrata, Washington is greatly appreciated.

8 REFERENCES

[1] National Research Council, “Upstream: Salmon and Society in the Pacific Northwest”, National Academic Press, Washington D.C. (1996)

[2] D.E. Weitkamp, “Hydraulic models as a guide to fish passage design”, Proc., Issues and Directions in Hydraulics. T. Nakato and R. Ettema eds., The University of Iowa, Iowa City, 287-293 (1995)

[3] E.A. Meselhe and F. Sotiropoulos, “Three-dimensional numerical model for open-channels with free surface variations”, *J. Hydr. Res*., **38**,115-121 (2000)

[4] C.S. Song and F. Zhou, “Simulation of free surface flow over spillway”, *J. Hydr. Eng*., **125**,959-967 (1999)

[5] B.M. Savage and M.C. Johnson, “Flow over ogee spillway: physical and numerical model case study”, *J. Hydr. Eng*., **127**, 640-649 (2001)

[6] C.W. Hirt and B.D. Nichols, “Volume of fluid (VOF) method for the dynamics of free boundaries”, *J. Comp. Phys*., **39**, 201-225 (1981)

[7] B.D. Nichols and C.W. Hirt, “Methods for calculating multi-dimensional, transient, free surface flows past bodies.” First International Conference on Numerical Ship Hydrodynamics, Bethesda, 253-277 (1975)

[8] Q. Chen, G. Dai and H. Liu, “Volume of fluid model for turbulence numerical simulation of stepped spillway overflow”, *J. Hydr. Eng.*, **128**, 683-688 (2002)

[9] Fluent 6.1 User’s Guide, Fluent Inc., Lebanon (2003)

[10] J.A. Sethian and P. Smereka, “Level set methods for fluid interfaces”, *Ann. Rev. Fluid Mech*., **35**, 341-372 (2003)